Percolation in aggregates of nanoclusters immersed in superfluid helium

S. Mao,[1,*] A. Meraki,[1] R. E. Boltnev,[2] V. V. Khmelenko,[1] and D. M. Lee[1]

[1]*Department of Physics and Astronomy and Institute for Quantum Science & Engineering, Texas A&M University, College Station, Texas 77843, USA*

[2]*Branch of Talroze Institute for Energy Problems of Chemical Physics, Russian Academy of Sciences, Chernogolovka 142432, Russia*

(Received 19 December 2013; published 3 April 2014)

Impurity-helium condensates created by injection of hydrogen (deuterium) atoms and molecules as well as rare gas (RG) atoms (Ne and Kr) into superfluid ^{4}He have been studied via electron spin resonance (ESR) techniques. Measurements of the ground-state spectroscopic parameters of hydrogen and deuterium atoms show that the nanoclusters have a shell structure. H and D atoms reside in solid molecular layers of H_2 and D_2, respectively. These layers form on the surfaces of RG (Ne or Kr) nanoclusters. By monitoring the recombination of H atoms in the collection of hydrogen-neon nanoclusters, we show that nanoclusters form a gel-like porous structure which enables the H atoms to be transported through the structure via percolation. Observation of percolation in the collection of nanoclusters containing stabilized hydrogen atoms may open possibilities for a search for macroscopic collective quantum phenomena at ultralow temperatures accessible by a dilution refrigerator.

DOI: 10.1103/PhysRevB.89.144301 PACS number(s): 66.30.Pa, 67.80.−s, 76.30.Rn, 61.46.−w

I. INTRODUCTION

The investigation of H atoms in a molecular H_2 matrix is a promising area of research. H atoms can move through solid H_2 via the tunneling exchange reaction $H + H_2 \rightarrow H_2 + H$ [1–4]. This phenomenon gives rise to the delocalization of H atoms and it opens up the possibility for the observation of quantum phenomena. For the observation of collective quantum phenomena, the thermal de Broglie wavelength must be longer than the distance between H atoms. High concentrations of H atoms and low temperatures are essential for this criterion to be satisfied. Unfortunately the same exchange reaction can lead to a recombination driven decay of the H atom concentration at $T \geqslant 1$ K [4]. Recently it was found that decreasing the temperature to 150 mK leads to significant suppression of the H atom recombination process [5]. This makes a search for quantum phenomena possible in systems with high concentrations of H atoms at low temperatures in thin and thick H_2 films [5–8]. Unusual behavior of H atoms in H_2 films was found at temperatures ∼150 mK. The significant departure from the Boltzmann distribution of the relative populations of the two lowest hyperfine levels of H atoms was observed [5] at atom concentrations $\sim 10^{18}$ cm^{-3}. A complete explanation of this effect will require additional experiments at higher H atom concentrations to test the quantum overlap hypothesis and to observe additional quantum effects.

Impurity-helium condensates (IHCs) consist of nanoscale clusters which adhere together to form a gel-like solid [9–12]. Each cluster is coated with a thin layer of solid helium which greatly retards the recombination of the stabilized atoms. IHCs are the best candidates for achieving record high concentrations of stabilized atoms [13–15]. The highest average ($\sim 10^{19}$ cm^{-3}) and local ($\sim 6 \times 10^{19}$ cm^{-3}) concentrations of H atoms were obtained in H_2 films formed in hydrogen-krypton helium samples [15]. The existence of a layer of H_2 molecules covering the Kr nanocluster surface provides an arena for the study of the diffusion and tunneling of H atoms [15]. To observe macroscopic quantum effects in this system, it is important to determine whether or not the H atoms can move relatively freely between the nanoclusters. This process is known as percolation and is an important feature for observation of macroscopic quantum overlap phenomena in impurity-helium condensates containing high concentrations of stabilized H atoms.

In this work, we present experimental studies for percolation between nanoclusters in IHCs containing stabilized H and D atoms. Our approach is based on the observation of H atom recombination or exchange tunneling reactions between atoms and molecules of hydrogen isotopes from neighboring nanoclusters in the IHC samples using the electron spin resonance (ESR) technique. H and D atoms each exhibit a different ESR spectrum, which makes it straightforward to study the kinetics of the reactions involving these atoms. We studied percolation for two different types of IHCs in our experiments.

First, we studied the possibility of the transfer of H atoms between nanoclusters in hydrogen-neon-helium condensates. For this purpose, we prepared IHC samples in which the number of stabilized H atoms was less than the number of nanoclusters in the sample, and studied the process of H atom recombination in these samples. We found that the recombination process continues even when the number of H atoms is five times less than the number of nanoclusters. This observation provides strong evidence for percolation between nanoclusters in hydrogen-neon-helium condensates.

Second, we studied the possibility of observing the transfer of D atoms in the layered IHCs in which layers of D-D_2 nanoclusters alternate with layers of H_2-Ne or H_2-Kr nanoclusters. If D atoms migrate to neighboring nanoclusters, the exchange tunneling chemical reactions with H_2 molecules should lead to increasing concentrations of H atoms in the samples, which can be easily observed by ESR. In as-prepared layered samples we did not observe any evidence for D atoms traveling between nanoclusters. Annealing of the layered samples to 2.6 K results in the onset of the exchange tunneling reactions, providing evidence of apparent connections between nanoclusters in these layered samples.

*maoshunghost@tamu.edu

II. EXPERIMENTAL METHOD

The experimental setup for investigating stabilized atoms in IHCs at low temperatures has been described in more detail elsewhere [14,16]. The experiments were performed in a specially designed Janis cryostat with a variable temperature insert (VTI), which is a separate chamber, thermally insulated from the main 4 K helium bath. A needle valve connects the main helium bath of the cryostat to the VTI. Pumping on the VTI, while supplying liquid helium from the main bath, permits long-term investigations of impurity-helium condensates at temperatures above 1.2 K. The lower part of the cryostat was placed between the pole pieces of a homogeneous Varian electromagnet for CW ESR investigations. IHCs with stabilized atoms for ESR investigations were prepared *in situ* in the Janis cryostat. A homemade insert for formation and investigation of atoms contained in IHCs was used in this work [17]. For sample preparation, a gas mixture of $H_2(D_2)$, rare gas (RG) Ne(Kr), and He was transported from a room temperature gas handling system to the cryogenic region. To provide the H and D atoms via dissociation of the molecules in gas phase, high-power radio frequency ($f \sim 50$ MHz, $P \sim 70$ W) was applied to electrodes placed around the quartz capillary carrying the mixed gases. The resulting jet of helium gas with a small fraction (0.5%) of impurity atoms and molecules emerging from the quartz capillary was directed onto the surface of superfluid ^{4}He contained in a small beaker suspended above the VTI main helium bath. The addition of helium gas increased the efficiency of dissociation of impurity molecules in the discharge due to interaction between the impurity and metastable He atoms, and also retarded agglomeration of impurity atoms and molecules in the gas jet. The jet penetrated the surface of the liquid helium and a macroscopic snow-like translucent material was created. This material fell down through the liquid ^{4}He to form a porous solid at the bottom of the beaker. A fountain pump connected to the bottom of the main helium bath in the VTI maintained a constant liquid helium level in the beaker. The temperature during sample preparation was 1.5 K. At the top of the beaker was a funnel that caught the sample as it condensed below the helium surface, which was 2 cm below the end of the quartz capillary. A set of Teflon blades scraped the sample from the funnel while the beaker was rotated so that the sample could fall to the bottom of the narrow cylindrical part of the beaker [18]. A jet with a total flux of $\sim 5 \times 10^{19}$ atoms and molecules per second yields $\sim$0.3–0.4 cm^3 of sample in 10 minutes.

After sample preparation, the beaker containing the sample was lowered into the ESR cavity through a hole in the cavity specially designed to fit the lower, cylindrical part of the beaker [see Fig. 1(a)]. The homemade cylindrical cavity [18] was operated in the TE_{011} mode and was situated at the bottom of the cryostat in the homogeneous field region of the Varian 7800 electromagnet. The quality factor of the cavity was equal to 3000. The volume occupied by the sample inside the cavity was 0.35 cm^3. The position of the beaker in the cavity and the dependence of ESR signal sensitivity on height are shown in Fig. 1. CW ESR signals were obtained for samples immersed in liquid helium at temperatures $\sim$1.35 K, and they were recorded by a continuous wave reflection homodyne spectrometer (Bruker E300) operating at an X-band

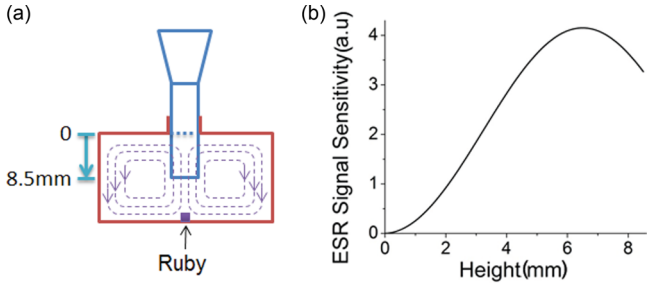

FIG. 1. (Color online) The position of the beaker in the ESR cavity (a) and the dependence of ESR signal sensitivity on height (b). The dotted lines with arrows in figure (a) show the microwave magnetic field distribution in the cavity operated in TE_{011} mode.

microwave frequency near 8.93 GHz. Derivatives of the ESR absorption lines were detected at $\sim$0.32 T by lock-in amplification using an additional small amplitude modulation field oscillating at 100 kHz. The number of atoms studied was measured by comparing the intensity of the atomic signals with the intensity of a signal from a small ruby crystal that was used as a secondary standard. The ruby crystal was attached permanently to the bottom of the microwave cavity [see Fig. 1(a)]. The calibration of the absolute value of the number of spins in the ruby crystal was made by using a standard organic diphenyl-picrylhydrazil (DPPH) sample with a known number (2.4×10^{17}) of spins. The atomic concentrations was calculated by dividing the number of atoms by the volume of the sample. A nuclear magnetic resonance (NMR) magnetometer was used for precise measurements of the applied magnetic field. The microwave carrier frequency was precisely measured by using a frequency counter EIP 545B from Phase Matrix Inc. while the field was swept through the resonance.

III. EXPERIMENTAL RESULTS

A. Studies of condensates formed by H-H_2-Ne-He nanoclusters

We performed long term (up to 10 hours) ESR investigations of the three samples formed by injecting the gas mixture [H_2]:[Ne]:[He] = 4:1:500 into He II. The structure of the samples is illustrated in Fig. 2(a). Two samples (A1 and A3) were prepared by using the discharge during the period of sample accumulation. The radio-frequency discharge provided the atomic hydrogen through dissociation of H_2, and soon afterward the H atoms were captured by nanoclusters growing in the cold helium gas jet. The H-H_2-Ne-He nanoclusters were then collected at the bottom of the quartz beaker for ESR registration of H atoms. If the mixture is passed through the capillary without discharge, we should not expect the presence of free H atoms in the sample. On the other hand, if the discharge is on throughout the sample preparation, the H atoms should be uniformly distributed in the sample as shown in Fig. 2(a) (left). Figure 2(a) (right) illustrates the situation for which the lower part of the sample is prepared without discharge, and the upper part of the sample is accumulated when the discharge was running. Thus, in sample A2, only in the top half of the sample are the H atoms present, and

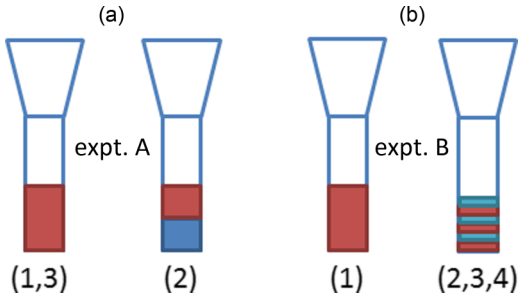

FIG. 2. (Color online) The position of the samples in the beaker and the structure of the samples. In experiments A the gas mixture used was $[H_2]$:[Ne]:[He] = 4:1:500. In experiment A1 and A3 all samples were prepared by passing the entire condensing gas mixture through the discharge zone. In experiment A2 the lower part of the sample was prepared without discharge action. The gas mixtures used in experiments B are $[D_2]$:[He] = 1:100 for the red layers of B1, B2, B3 and $[D_2]$:[He] = 1:25 for the red layer of B4 with discharge action; the mixtures for blue layers for B2, B3 and B4 are $[H_2]$:[Kr]:[He] = 1:5:150, $[H_2]$:[Ne]:[He] = 1:5:150, and $[H_2]$:[Ne]:[He] = 1:5:150, respectively, *without* discharge action.

in the bottom half initially H atoms are absent. Figure 3 shows the ESR spectra from the first sample (A1) at the beginning of experiments, after 4 h, and after 8 h. The ESR spectra from other two samples (A2, A3) are very similar. The two main signals correspond to the atomic hydrogen low-field and high-field lines separated by 508.7 G. Each main line is accompanied by two satellite lines, which result from the forbidden transitions involving an electron spin flip of an H atom and a simultaneous spin flip of a proton on a neighboring ortho-H_2 molecule [19]. The splitting observed between the left main line and satellite lines is 4.6 ± 0.1 G, while that between the right main line and the satellite lines is 5.3 ± 0.1 G.

The three spectra of Fig. 3 for sample A1 shows a significant decrease of intensity over an eight hour period. The intensities

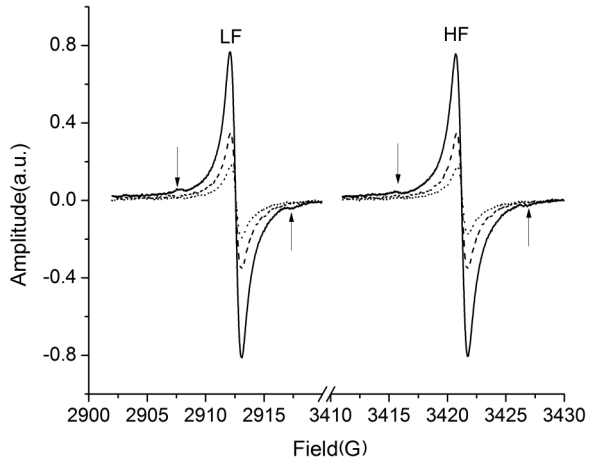

FIG. 3. The ESR spectra of H atoms in sample A1 showing the high-field and low-field lines for an as-prepared sample (solid), after a waiting time of 4 h (dashed), and after a waiting time of 8 h (dotted). The arrows show the satellite lines associated with nuclear spin flips on ortho-H_2 molecules [19].

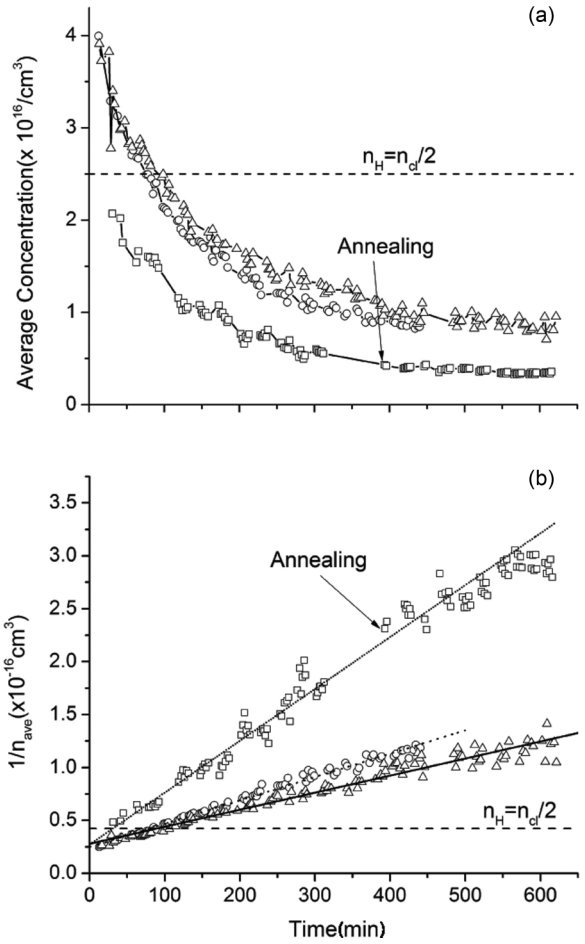

FIG. 4. The dependence of the average concentration (a) of H atoms and its reciprocal $1/n_{\rm ave}$ (b) on time for samples A1 (open circles), A2 (open triangles), and A3 (open squares). Only sample A3 was annealed at $t = 400$ min. The dashed flat line shows the expected plateau level for disconnected clusters. The short-dotted, solid, and long-dotted lines in (b) are the linear fitting lines for samples A1, A2, and A3, respectively.

of both the high-field (HF) and low-field (LF) ESR lines of hydrogen are reduced by a factor of 4 as compared to the signal for the initially prepared samples. This decline results from the process of recombination of H atoms. The reaction

$$H + H_2 \rightarrow H_2 + H \qquad (1)$$

allows the H atoms to move through the sample until they encounter other hydrogen atoms at which point recombination can occur, according to the reaction

$$H + H \rightarrow H_2. \qquad (2)$$

The barely visible satellite lines in the last measured ESR spectrum indicate ortho-para conversion of H_2 molecules surrounding H atoms during the course of the experiment.

The dependence of the average concentration of H atoms in each of the three samples (1, 2, and 3) on time is illustrated in Fig. 4(a). The initial average concentration of H atoms in each sample is in the range (2–4) $\times 10^{16}$ cm^{-3}. During decay, the concentration of H atoms decreased to approximately 1/4 of the initial value. This clearly shows the result of H atom

TABLE I. The recombination rate of H atoms for the three different H-H_2-Ne-He samples.

Sample	Calculated k_H at 1.35 K ($cm^3 s^{-1}$)
A1	1.83×10^{-23}
A2	1.50×10^{-23}
A3	4.08×10^{-23}

recombination in the collection of nanoclusters. Furthermore, as discussed below, since the cluster concentration is much greater ($n_{cl} = 5 \times 10^{16}$ cm^{-3}, see Discussion section) than the stabilized H atom concentration, percolation through the collection of nanoclusters must take place to allow a hydrogen atom to find a partner. The equation

$$\frac{dn_H}{dt} = -2k_H(T)n_H^2 \tag{3}$$

describes the decrease of the local concentration of H atoms (n_H) with time when the temperature of the sample is kept constant. The experimental dependence of the reciprocal concentration ($1/n_H$) on time should thus be linear, with slope equal to $2k_H(T)$. Figure 4(b) shows the dependence of $1/n_{ave}$ on time for each of these samples. From a previous ESR and x-ray study [9–11] we know that, in impurity-helium condensates formed with H_2 molecules and Ne atoms, the local concentration of H atoms inside nanoclusters is roughly two orders magnitude larger than the measured average concentration. So, based on this fact and a linear fitting to the slope of each line, we can calculate the recombination rate of H atoms at $T = 1.35$ K, which is shown in Table I. The estimated recombination rates are in good agreement with those obtained by the Nagoya group, $k_H(1.9–4.2\ K) = (4.4–5.9) \times 10^{-23}$ cm^3 s^{-1} for bulk solid hydrogen samples irradiated by γ rays [20].

The actual rate of spatial diffusion of H atoms in the H_2 crystal is at least three orders of magnitude greater than that estimated from the recombination rate of H atoms [21]. Therefore, it should be possible to observe such rapid spatial diffusion of H atoms from the region in the sample with high concentration of H atoms to the region where H atoms are absent in a specially designed sample. The sample A2 was divided in half with the bottom half containing no H atoms due to the accumulation of this part of sample without discharge, and the top half containing H atoms as a result of preparing with the discharge. If the entire sample created is percolated due to the rapidly repeating chemical tunneling reaction (1), we should expect that the H atoms should also be able to move into the lower half. Since in our cavity the space in the bottom half of the beaker has a 2.2 times larger ESR signal sensitivity [see Figs. 1(a) and 1(b)], after a period of time the ESR signal from atoms in the lower half should grow and the overall decay of H atoms in the whole sample should be seen as a slower process compared to that in sample A1. From Fig. 4(a) we see that, from the start of observation, samples A1 and A2 have almost the same rate of decrease from the initial average concentration, but after about 200 min data for A2 starts to deviate from that of A1 and show a somewhat smaller recombination rate in Fig. 4(b). This could be the direct evidence that the H atoms migrate from cluster to cluster and try to diffuse to the bottom half of the sample.

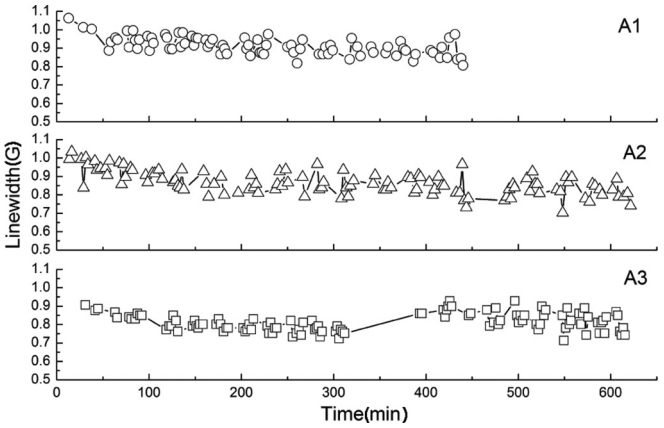

FIG. 5. Dependence of ESR signal linewidths of H atoms for sample A1 (open circles), A2 (open triangles), and A3 (open squares) on time.

Sample A3 initially had a smaller concentration compared to that of samples A1 and A2. Also the recombination rate for this sample was 2–2.5 times larger than that for the A1 and A2 samples. We performed annealing of sample A3 after 400 min of observation. During the annealing, the sample temperature was gradually increased from 1.35 to 2.6 K. After that the sample was kept out of liquid helium for about 30 mins at $T = 2.6$ K and then cooled down with liquid helium back to 1.35 K. The behavior of the average concentration before and after annealing is more or less the same as for the unannealed samples without showing any additional increase or decrease of the quantity of H atoms. However, it is clearly seen that in Fig. 4(b) the experimental value starts to deviate from the fitted line at about 500 min and tends to be more stable. The recombination rate of H atoms therefore seems to be reduced significantly in the last 100 min of observation, as evidenced by the change in slope.

During the course of observation of the ESR signals of H atoms, their linewidths decreased. Figure 5 shows the dependence of the ESR signal linewidths of H atoms on time for the three samples. The initial linewidths of the H atoms are in the range 0.91–1.06 G, which are in good agreement with the previous result for the case of H atoms in an initially normal H_2 matrix [22]. During the observation time, the linewidth decreases almost linearly indicating catalyzed ortho-para conversion of H_2 molecules. Assuming a linear fitting, we can calculate the rates of decrease for the linewidths, which are 2×10^{-4} G/min for the samples A1 and A2 and 4×10^{-4}G/min for A3. For sample A3, the annealing process led to the sudden increase (∼15%) of the linewidth which could be a result of an increase of the local concentration of H atoms. After annealing, the linewidth again starts to decrease with almost the same rate.

The low- and high-field spectra of H atoms in H_2-Ne-He samples were each fitted with a Lorentzian line. The results of the analysis are shown in Table II, where we list the values of the g factors and the hyperfine structure constants, A, obtained for H atoms from the experimental data for H-H_2-Ne-He samples. The data for H atoms in the gas phase, in solid H_2 and

TABLE II. Hyperfine structure constants, A, and g factors of H atoms in H-H_2-Ne-He samples, in the gas phase, in solid H_2 and in Ne matrices.

Sample	A (MHz)	$\Delta A/A_{\text{free}}$ (%)	g factor
A1	1416.82(6)	−0.25	2.00242(6)
A2	1416.84(8)	−0.25	2.00242(5)
A3	1416.95(3)	−0.24	2.00242(2)
Gas phase [24,25]	1420.40573(5)	0	2.002256(24)
H_2 [23]	1417.13(45)	−0.23	2.00243(8)
Ne (subst.) [26]	1426.51(3)	0.43	2.00206(6)

in Ne matrices are also listed in Table II for comparison. The spectroscopic characteristics of H atoms in the H-H_2-Ne-He samples are very similar to those obtained for H atoms in an H_2 matrix [23]. This observation is consistent with the shell model of the nanoclusters which form the impurity-helium condensates [15]. The H atoms are trapped in layers of solid H_2 which covered the surfaces of Ne cores of the clusters (see Fig. 6). The influence of the Ne atoms in the core on the spectroscopic characteristics of H atoms is minimal due to the formation of thick layers of H_2 molecules as a consequence of the large ratio $H_2/Ne = 4$ in the condensed gas mixture.

B. Studies of condensates containing alternate layers of D-D_2-He and H_2-RG-He nanoclusters

For observation of possible migration of D atoms from one type of nanocluster to the H_2 molecule layers in another type of nanocluster, we also studied samples in which layers of D-D_2-He nanoclusters were separated by layers of H_2-Ne-He (or H_2-Kr-He) nanoclusters. Each layer of the sample was prepared during 2 min of condensation of the appropriate gas mixture and collected in the cylindrical part of the beaker [see Fig. 2(b)]. In this set of experiments, the D_2-He mixtures were passed through the discharge zone in order to create D atoms while the H_2-Ne-He or H_2-Kr-He gas mixtures were injected into the He II without action of the discharge so as to store H_2 molecules in the sample. In this approach we might expect

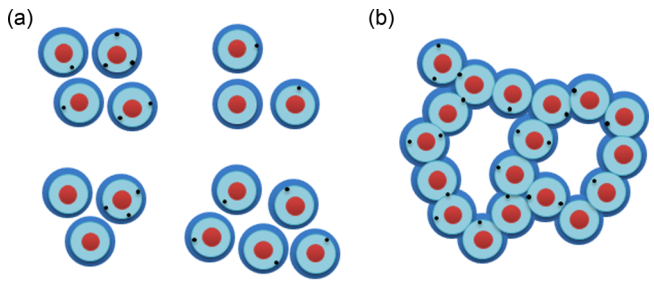

FIG. 6. (Color online) Two possible cases for collection of nanoclusters immersed in bulk superfluid helium. (a) Collection of separated nanoclusters. (b) Percolated aggregates of nanoclusters. The lighter shaded areas correspond to the lighter impurity layers (H_2 or D_2) and the central dark discs are the heavier impurity cores (Ne or Kr); the outer rings correspond to the solid helium layers covering the nanoclusters; black dots are free atoms (H or D) embedded on the surface of the nanoclusters.

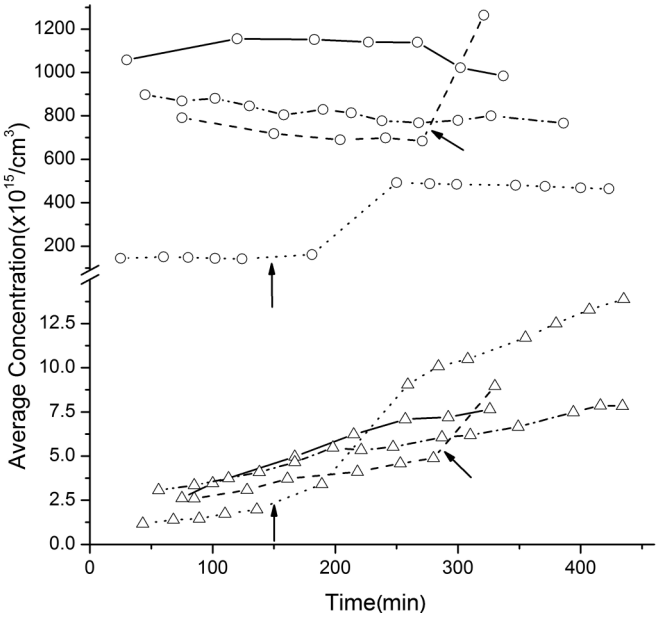

FIG. 7. The time dependence of average concentration of D atoms (open circles) and H atoms (open triangles) in samples B1 (dashed line), B2 (solid line), B3 (dotted line), and B4 (dash-dotted line). The arrows show times for starting annealing of the samples: B1 (288 min) and B3 (150 min).

that, at the beginning of the experiment in the mixed sample, only an ESR signal from D atoms should be present. In the case of percolation between nanoclusters from different layers we can expect an observation of the rather fast chemical reaction

$$D + H_2 \rightarrow H + HD \quad (4)$$

leading to an increase of the signal from the H atoms in the sample and a decrease of the signal from the D atoms. However, for all layered samples, we observed strong ESR signals for D atoms together with a weak signal for H atoms even at the onset of observations. The presence of H atoms in the samples was due to the small impurity(0.4%) of HD molecules in the Matheson D_2 gas, which we used in our experiments. That is why sample B1, which nominally contains only D-D_2-He nanoclusters, was prepared to compare the behavior of the changing H and D concentration in this sample with that in the layered samples.

Figure 7 illustrates the dependence of the average concentrations of both D and H atoms on time for each of the samples studied. The four samples show very similar rates of decay of D atoms and the increase of H atoms. This gives evidence that the following reactions occurred in the samples:

$$D + D \rightarrow D_2 \quad (5)$$

$$D + HD \rightarrow H + D_2 \quad (6)$$

Previous experimental studies [27] have shown that the rate constant for reaction (5) is about one order of magnitude larger than for reaction (6). Therefore, the decay of D atom concentrations is determined mostly by reaction (5), while the relatively small increase of H atom concentration and a

TABLE III. Concentration and rate constants of each sample.

Sample	Initial n_{ave}, (cm^{-3})		Rate constants (cm^3s^{-1})	
	D atoms	H atoms	k_D	$k_{D\text{-}HD}$
B1	7.92×10^{17}	2.60×10^{15}	8.05×10^{-26}	2.57×10^{-27}
B2	1.06×10^{18}	2.62×10^{15}	5.71×10^{-26}	3.28×10^{-27}
B3	1.45×10^{17}	1.17×10^{15}	5.74×10^{-26}	9.68×10^{-27}
B4	8.90×10^{17}	3.07×10^{15}	4.67×10^{-26}	2.45×10^{-27}

corresponding small decrease of D atom concentrations is provided by reaction (6). Since this behavior was observed even in sample B1 prepared purely from the nominal D_2-He gas mixture, it was clear that HD molecules were present in this sample as a result of the presence of a small impurity of HD molecules in the D_2 gas used in the experiments. Due to the similar behavior of the kinetics of D and H atoms in layered samples and in the D-D_2-He sample, we can conclude that we do not obtain direct evidence for fast reaction (4) in the layered samples B2, B3, and B4 from these experiments. The only processes observed in those samples are occurring in the D-D_2-He layers. Otherwise, we should have observed an enhancement of H atom concentrations in these layered samples as compared with those in the D-D_2-He samples. Table III shows the initial concentrations of both D and H atoms as well as the rate constants for reaction (5) and (6) in each sample studied. The estimated k_D and $k_{D\text{-}HD}$ are in agreement with the results of previous work [27].

Table IV is a summary of the hyperfine structure constants, A, and g factors for ESR spectra of H and D atoms in layered and D-D_2-He samples. The values of A and g in the gas phase as well as in solid H_2, D_2, Ne, and Kr matrices are also given for comparison. In all samples studied in the experiments, the g factors and hyperfine constants of D atoms are closest to the values for a D_2 matrix, which is naturally reasonable due to

TABLE IV. Hyperfine structure constants, A, and g factors for ESR spectra of H and D atoms in layered samples, in D-D_2-He samples, in the gas phase, and in solid H_2 and D_2 matrices.

Atoms, sample	A (MHz)	$\Delta A/A_{free}$ (%)	g factor
H, B1	1416.42(2)	−0.28	2.00225(3)
H, B2	1416.71(4)	−0.26	2.00226(9)
H, B3	1416.53(4)	−0.27	2.00215(6)
H, B4	1416.56(7)	−0.27	2.00218(4)
H, gas phase [24,25]	1420.40573(5)	0	2.002256(24)
H, H_2[23]	1417.13(45)	−0.23	2.00243(8)
H, Kr (subst.) [26]	1411.799	−0.61	2.00179(8)
H, Kr (subst.) [28]	1409	−0.80	2.0013
D, B1	217.663(8)	−0.27	2.00219(6)
D, B2	217.656(4)	−0.27	2.00220(3)
D, B3	217.659(6)	−0.27	2.00220(4)
D, B4	217.641(6)	−0.28	2.00219(9)
D, gas phase [29,30]	218.25601	0	2.002256
D, D_2 [31]	217.71(18)	−0.25	2.00231(8)
D, D_2 [32]	218.86(15)	−0.28	2.00220(16)
D, Kr (subst.) [33]	216.30	−0.896	2.0015
D, Ne (subst.) [33]	219.0(1)	0.345	2.0020(1)

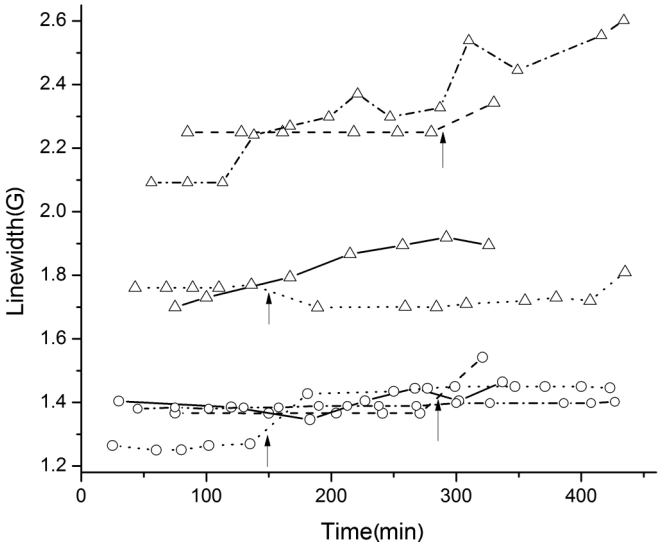

FIG. 8. The time dependence of linewidth of D atoms (open circles) and H atoms (open triangles) in samples B1 (dashed line), B2 (solid line), B3 (dotted line), and B4 (dash dotted line). The arrows show times for starting annealing of the samples: B1 (288 min) and B3 (150 min).

the mixture we used. For H atoms, the g factors are slightly smaller than those in an H_2 matrix. We think that H atoms should exist in the environment of D_2 molecules because of the low average concentration of H atoms. However, we were not able to find any reference containing hyperfine constant and g factor values of H atoms in a D_2 matrix to compare with. Figure 8 shows the time dependence of the linewidths of D atoms and H atoms in the samples. The main fact in Fig. 8 is that the linewidths of H atom signals (1.7–2.6 G) are significantly larger than that for D atoms (1.2–1.4 G). Also, the linewidths of H atoms in mixed samples are higher than those for H atoms in an H_2 matrix (1–0.8 G). Miyazaki *et al.* [34] have shown that H and D atoms in solid HD and D_2 are trapped in interstitial octahedral sites, while H atoms in solid H_2 are trapped in the substitutional sites. Therefore, H atoms in solid H_2 are trapped in larger sites than D atoms in solid D_2, corresponding to the longer distance between a trapped H atom and nearest-neighbor molecules in solid H_2. Thus, the superhyperfine interaction in solid H_2 is weaker than that in solid D_2, resulting in a narrower spectrum of H atoms in H_2. However, this could not explain why the linewidths of H atoms are larger than those for D atoms in a D_2 matrix. The explanation will be given later.

More promising results were observed for annealed samples. The annealing was employed for samples B1 and B3 (see Figs. 7 and 8). After annealing the samples to 2.6 K and cooling back to 1.35 K, the average concentration of both D atoms and H atoms increased by a few times due to the compressing of the samples and collapsing pores. The elimination of the pores reduces the volume of the sample. If most of the H atoms survive during annealing, their average concentrations should increase. Table V shows the average concentrations of H and D atoms and their ratio just before and after the annealing process. We can see from the Table V

TABLE V. Average Concentrations of H and D atoms before and after annealing of the samples B1 and B3

	B1		B3	
Sample	D atoms	H atoms	D atoms	H atoms
Before annealing, n_0	6.84×10^{17}	4.88×10^{15}	1.42×10^{17}	1.97×10^{15}
After annealing, n_{ann}	1.26×10^{18}	8.96×10^{15}	4.93×10^{17}	9.04×10^{15}
Ratio, n_{ann}/n_0	1.85	1.84	3.47	4.59

that for sample B1 the concentrations of both D and H atoms were increased by the same factor, about 1.84 times after annealing, while for sample B3 the H atom concentration increased more than that for D atoms. This result indicates that, in the sample B1, only the effects of increasing the average concentrations of H and D atoms due to collapsing pores were observed. In sample B3, in addition to the simultaneous increase of both concentrations of H and D atoms due to the collapsing pores in the sample (∼3.47 times), an extra increase in concentration of H atoms was observed, which could not be explained by reaction (6) which has a rather small rate constant and during annealing time (∼40 min) could not make substantial changes of H and D concentration. Therefore, the most plausible explanation is that the annealing process also helped to create paths available for D atoms to meet H_2 molecules. In this case, due to the fast reaction (4), more H atoms were produced. This annealing process has convinced us of the possibility of creating percolation in the samples composed of nanoclusters containing mixtures of hydrogen isotopes. More evidence for percolation was also found in the linewidth study during the annealing process. For sample B1, the annealing was performed before the last measurement, which resulted in the line broadening of both H and D atom signals. This can be explained by the increase of the local concentration of both H and D atoms and thus by the enhanced electron spin dipole-dipole interaction. However, for sample B3, the annealing did not have the same effect on H and D atoms. Instead, the linewidth of H atoms shows a slight decrease while that of D atoms still increased. This might support the idea of percolation in which the new H atoms produced as a result of annealing are not in the same environment as H atoms already in place.

IV. DISCUSSION

Impurity-helium condensates are porous gel-like materials created by injecting a mixed beam of helium gas and some impurity atoms and molecules into superfluid helium [9–11]. The collection of nanoclusters formed by impurities creates a porous structure with nanoscale pores inside He II [10,35,36]. Isolation of highly reactive atoms in nanoclusters surrounded by He II leads to the stabilization of high concentrations of these atoms [14,15]. In the case of injection of two different impurities into He II, the nanoclusters have shell structures in which heavier impurities form cores surrounded by lighter impurities plus solid helium. In experiments involving hydrogen-krypton-helium jets, high average and local concentration of H atoms were achieved [15]. These H atoms are stabilized in the H_2 films which cover the Kr cores of nanoclusters. The existence of a layer of H_2 molecules covering a Kr cluster surface provides an environment which allows the study of the diffusion and tunneling of H atoms. In this environment, samples containing high concentrations of H atoms may exhibit interacting macroscopic Bose-Einstein correlations at lower temperatures if H atoms can travel rather freely between H_2 layers of different nanoclusters. This requires that the thermal de Broglie wavelength be comparable or greater than the average spacing between H atoms. Hence investigation of the possibility of transport of atoms of the light hydrogen isotopes between nanoclusters at lower temperatures in impurity-helium condensates is of great interest. Experiments by Reppy and coworkers have demonstrated Bose-Einstein correlations for very dilute films of liquid helium trapped in porous vycor glass [37,38].

In hydrogen-krypton samples prepared from a $[H_2]$:[Kr]:[He] = 1:1:200 gas mixture, the average concentration of H atoms $n_H = 1.4 \times 10^{18}$ cm^{-3} was obtained [15]. According to x-ray investigations [12] the average density of impurities in these samples is of order 10^{20} cm^{-3} and the number of impurities in a cluster with diameter 5 nm is equal to ∼2000. This information allows one to calculate the concentration of clusters in the sample, $n_{cl} = 5.0 \times 10^{16}$ cm^{-3} and make an estimate of the number of H atoms in each of the clusters, $n_H = 28$ per cluster. Therefore, during studies of the recombination of H atoms in samples with high concentrations of atoms, it is difficult to distinguish processes occurring inside the clusters from those occurring between clusters. The lifetime for decay of H atoms in this sample was ∼160 min [15]. Achieving a regime when only a single H atom is stabilized in a cluster [39,40] allows one to monitor the process of recombination of H atoms from different clusters. For the above-mentioned hydrogen-krypton samples, this requires continuation of experiments after observation times larger than 10 h. Therefore, in this work we used a different approach for studying percolation between nanoclusters. Instead, we initially created hydrogen-neon samples in which the number of stabilized H atoms are close to or even less than the number of clusters in the samples. From the spectroscopic characteristics of H atoms presented in Table II, we can conclude that these atoms are mostly stabilized in the H_2 layers formed on the surfaces of Ne nanoclusters. We have not observed signals which may be assigned to the H atoms stabilized in the Ne matrix. In this situation, even from the beginning of the investigation, we should observe recombinational decay of H atoms only if there are connections between nanoclusters [see Fig. 6(b)]. For the case of collections of nonpercolating clusters [see Fig. 6(a)], we should observe a plateau for $n_H = n_{cl}/2 = 2.5 \times 10^{16}$ cm^{-3}

on the dependence of H atom concentration on time. This value is calculated from considering the fact that in the clusters with even numbers of H atoms all atoms should eventually recombine, whereas in clusters with odd numbers of H atoms only one atom will remain per cluster. Initially on average half of the clusters should contain an even number of H atoms and other half should contain an odd number of H atoms.

Results presented in Fig. 4 show that recombination of H atoms continues even when the number of H atoms in the samples is much less than one half of number of clusters. These results provide strong evidence for percolation in the collection of hydrogen-neon nanoclusters. The success of this experiment resulted from the rapid process of chemical diffusion of H atoms due to the exchange tunneling reaction between H atoms and H_2 molecules. The spatial diffusion coefficient for H atoms in an H_2 matrix, $D_{sp} \geqslant 10^{-13}$ cm^2/s, is four orders of magnitude larger than that obtained from the H atom recombination process, $D_{\rm rec} = 10^{-17}$ cm^2/s [18,21]. The fast spatial diffusion allows H atoms to find a partner in the connected layers of solid H_2 matrix and recombine.

Completely different behavior was observed for layered samples. In the layers formed by a D-D_2-He gas mixture, the nanoclusters of D_2 contain stabilized D atoms mainly on their surfaces [41]. In layers formed by H_2-Ne-He or H_2-Kr-He gas mixtures, the H_2 layers formed on the surfaces of Ne or Kr nanoclusters. In either case, if the nanoclusters from different layers are connected, we would expect to observe a rather fast (a few minutes) reaction (4) of D atoms with the H_2 molecules [42,43]. From the comparison of the processes of D atom recombination and production of H atoms in the pure D-D_2-He sample and in the layered samples (see Fig. 8), we did not find any direct evidence for the percolation between nanoclusters. The dynamics of changes of D and H atom concentrations in those samples were similar. Only annealing of the layered samples gave evidence for enhancement of H atom concentrations and correspondingly for percolation in these samples. The absence of obvious effects of enhancing H atom concentrations in layered samples does not rule out the possibility of percolation in those samples. The recombination of D atoms with H_2 molecule occurs only when these species are in neighboring sites in a solid matrix. This means that D atoms should move to a position adjacent to a hydrogen molecule. The process of tunneling of D atoms through a D_2 matrix is four orders of magnitude slower compared with the rate of tunneling H atoms in an H_2 matrix [42]. Because of this very slow process for migration of D atoms we have not observed the enhancement of the concentration of H atoms in layered samples. Only sample annealing involving the collapsing of the pores can produce additional points of contact between clusters where D atoms and H_2 molecules could interact occasionally, resulting in the tunneling reaction, which leads to an increase of H atom concentration.

The rapid spatial migration of H atoms in an H_2 matrix helped us to observe changes in the distribution of H atoms with time in the presence of a gradient in H atom concentration in sample A2. In the lower part of the sample, which occupied the most sensitive region of the cavity, initially the hydrogen-neon sample did not contain H atoms. The volume above was filled with a hydrogen-neon sample which did contain H atoms. Luckily the concentration of H atoms in this sample was similar to that of another sample in which the H atoms were distributed throughout the entire sample (A1). If both samples are allowed to percolate and the rate of recombination of H atoms is comparable, we should observe decreasing decay in the sample with the H atom gradient due to the process of migration of H atoms from top of the sample to the bottom where the sensitivity of the signal is higher. This is exactly what we observed from a comparison of the decay of H atom concentrations in these samples. In the first 200 min of the experiment the points for samples A1 and A2 almost coincided (see Fig. 4). However, after this period, the effective decay of H atoms in the sample with a gradient of H atoms became slower. This observation clearly supports the existence of percolation between nanoclusters and effective transport of H atoms from the region containing nanoclusters with stabilized H atoms to the region with nanoclusters containing only layers of H_2 molecules.

Differences in initial concentrations of H and D atoms in different samples (see Fig. 4 and 6) could perhaps be explained by poor reproducibility of conditions in the discharge zone during the process of sample preparation. The observed ranges in the rates of H atom recombination in hydrogen-neon samples (see Table I) $(1.5–4.8)\times10^{-23}$ cm^3/s and D atom recombination in the layered samples $(4.67–8.05)\times10^{-26}$ cm^3/s (see Table III) might be related to different ortho-para ratios of H_2 and D_2 molecules, respectively [44]. The linewidths of H atoms in as-prepared H_2-Ne samples are of order 1 G and have a tendency to decrease as time progress. The concentrations of H atoms in these samples are rather small, so therefore electron spin dipole-dipole interactions do not contribute significantly to the broadening of the ESR lines. The broadening results from the interactions of electron spins of H atoms with nuclear spins in neighboring ortho-H_2 molecules. The decrease of the linewidths of H atoms with time might be explained by the slow ortho-para conversion of H_2 molecules at distances larger than the first coordination sphere surrounding each of the H atoms. The nearest-neighboring ortho-H_2 molecules are converted into para-H_2 molecules very rapidly ($\tau = 10$ s) [45,46]. The rate of decrease of the linewidths [$(2–4) \times 10^{-4}$ G/min] in our experiments are very similar to those observed in earlier experiments in which stabilized nitrogen atoms were added to the H_2 matrix [47].

In the layered samples and in the D-D_2-He sample, the linewidth of H atoms ($\sim$2 G) is larger than that for D atoms ($\sim$1.4 G). In both types of samples, most of the H and D atoms are stabilized in the D_2 matrix. In the D_2 molecular matrix the para state ($J = 1$) of D_2 molecules is 85 K more energetic than the ortho states of D_2 molecules ($J = 0,2$). The presence of H and D atoms in the D_2 matrix catalyzes the conversion from the para to the ortho state of D_2 molecules. The $J = 0$ ortho state must be accompanied by either the $I = 0$ or $I = 2$ spin sates. The $I = 2$ state is $2I + 1 = 5$ (fivefold degenerate), whereas the $I = 0$ state is nondegenerate. The energy splitting between the $I = 0$ and $I = 2$ states is negligible at liquid-helium temperatures, meaning that each of the five $I = 2$ states and the singlet $I = 0$ state are equally populated. As a result, a D atom on a substitutional site in an fcc D_2 matrix has 12 nearest-neighbor D_2 molecules in the first coordination shell, 10 of which correspond to spin $I = 2$. The increase in linewidth of the D atom in D_2 as compared to the linewdith of

H in H_2 is, therefore, due to the interaction of the electron spins of the D atoms with the nuclear spins of ortho-D_2 molecules having spins $I = 2$.

The even larger broadening of H atom ESR lines in a D_2 matrix can be explained by the larger zero-point energy of H atoms in comparison with stabilized D atom in a D_2 matrix. The electron spin interacts with the same number of ortho-D_2 molecules, but the larger amplitude of zero-point motion leads to an increase of the dipole-dipole interaction between the electron spin of H atoms and the nuclear spins of the ortho-D_2 molecules.

Based on the results of this work, we can conclude that it is possible to create hydrogen-RG-helium condensates which contain high concentrations of H atoms residing in the layers of H_2 molecules. The layers of H_2 molecules are percolated throughout the whole sample providing a unique system for studying quantum overlap effects of H atoms in the solid phase. For a H-H_2-Kr sample with a local concentration of H atoms $n_H = 6 \times 10^{19}$ cm^{-3} the mean distance between atoms in an H_2 layer is $d_m = 10^8$ Å$/\sqrt[3]{n_H} = 25$ Å. The thermal de Broglie wavelength $\lambda(T) = \sqrt{2\pi\hbar^2/mkT}$ for free H atoms will be comparable to the mean distance between atoms at $T = 484$ mK. The effective mass of H atoms in an H_2 matrix must be larger than that for free H atoms. But even if the effective mass of H atoms in H_2 is 10 times larger than that of free atoms, the temperature where the mean distance between H atoms is equal to the thermal de Broglie wavelength will be equal to ∼153 mK. This range of temperatures is easily accessible using a dilution refrigerator.

The process of formation and investigation of impurity-helium condensates is a challenging task. However, we are working on the design of the cell for creating and investigating impurity-helium condensates at temperatures below 1 K. The experiment setup will be similar to that used in experiments for studying H atoms in H_2 matrices [5–8] and spin-polarized atomic hydrogen gas [48] at ultralow temperatures. The modifications of the sample cell should allow filling it with superfluid helium and injecting the impurities into the superfluid helium at temperatures 0.5–0.7 K. The cell is thermally anchored to the dilution refrigerator mixing chamber. The sensitivity of the 130 GHz ESR spectrometer [5], which we plan to use in these experiments, is high enough for studying small quantities of the samples obtained during 10–20 min with a flux of 10^{16} impurity atoms and molecules per second. This regime has been successfully realized in our recent experiments by using a dilution refrigerator [49]. After finishing preparation, the sample can be cooled to 100 mK or lower.

V. CONCLUSIONS

The impurity-helium solids created by injection of hydrogen and deuterium atoms and molecules together with rare gas atoms (Ne or Kr) into superfluid helium have been studied by the ESR method. Processes of atomic recombination and exchange chemical tunneling reactions between atoms and molecules of hydrogen isotopes have been investigated at temperatures 1.35–2.6 K. Observations of H atom recombination have been performed in a situation for which the number of H atoms in the sample is less than the number of nanoclusters. It was shown for this case that H atoms could travel freely between clusters. This fact provides evidence for percolation between nanoclusters.

Measurements of ground-state spectroscopic parameters of hydrogen atoms provide clear evidence that nanoclusters have shell structures with the cores of hydrogen-neon nanoclusters formed by the heavier neon atoms and the outer layer formed by lighter hydrogen molecules in which most of H atoms are stabilized. These outer layers of the nanoclusters are connected, which allowed the H atom to travel via rapid spatial diffusion through the porous structure.

We observed a large isotope effect when we designed an experiment for the observation of an exchange tunneling reaction between D atoms on one cluster with H_2 molecules residing on another nanocluster. We did not observe the effect of an increasing concentration of H atoms expected from the tunneling exchange reactions between D atoms and H_2 molecules. This is a result of the very slow spatial diffusion of D atoms in a D_2 matrix.

Observation of percolation in aggregates of hydrogen-neon nanoclusters immersed in He II is an important step in the search for quantum correlation phenomena of H atoms in the solid phase at low temperatures. The combination of high concentrations of H atoms in H_2 layers on surfaces of Kr nanoclusters and the percolation of H atoms through the sample makes this system very attractive for the study of quantum overlap phenomena. The temperatures for the onset of possible quantum phenomena require a mean distance between H atoms in the system to be comparable to the thermal de Broglie wavelength of the H atoms. This temperature region should be accessible using a dilution refrigerator.

ACKNOWLEDGMENTS

This work was supported by NSF Grant No. DMR 1209255. We wish to thank Patrick McColgan and Trevor Dragon for participation in the experiments.

[1] H. Tsuruta, T. Miyazaki, and N. Azuma, J. Phys. Chem. **87**, 5422 (1983).

[2] S. I. Kiselev, V. V. Khmelenko, and D. M. Lee, Phys. Rev. Lett. **89**, 175301 (2002).

[3] T. Kumada, Phys. Rev. B **68**, 052301 (2003).

[4] T. Miyazaki, *Atom Tunneling Phenomena in Physics, Chemistry and Biology*, Springer Series on Atomic, Optical and Plasma Physics, Vol. 36 (Springer, Berlin, 2004).

[5] J. Ahokas, J. Jarvinen, V. V. Khmelenko, D. M. Lee, and S. Vasiliev, Phys. Rev. Lett. **97**, 095301 (2006).

[6] J. Ahokas, O. Vainio, J. Jarvinen, V. V. Khmelenko, D. M. Lee, and S. Vasiliev, Phys. Rev. B **79**, 220505 (2009).

[7] J. Ahokas, O. Vainio, S. Novotny, J. Jarvinen, V. V. Khmelenko, D. M. Lee, and S. Vasiliev, Phys. Rev. B **81**, 104516 (2010).

[8] J. Jarvinen, V. V. Khmelenko, D. M. Lee, J. Ahokas, and S. Vasiliev, J. Low Temp. Phys. **162**, 96 (2011).
[9] V. Kiryukhin, B. Keimer, R. E. Boltnev, V. V. Khmelenko, and E. B. Gordon, Phys. Rev. Lett. **79**, 1774 (1997).
[10] S. I. Kiselev, V. V. Khmelenko, D. M. Lee, V. Kiryukhin, R. E. Boltnev, E. B. Gordon, and B. Keimer, Phys. Rev. B **65**, 024517 (2001).
[11] E. P. Bernard, R. E. Boltnev, V. V. Khmelenko, V. Kiryukhin, S. I. Kiselev, and D. M. Lee, Phys. Rev. B **69**, 104201 (2004).
[12] V. Kiryukhin, E. P. Bernard, V. V. Khmelenko, R. E. Boltnev, N. V. Krainyukova, and D. M. Lee, Phys. Rev. Lett. **98**, 195506 (2007).
[13] E. B. Gordon, V. V. Khmelenko, E. A. Popov, A. A. Pelmenev, and O. F. Pugachev, Chem. Phys. Lett. **155**, 301 (1989).
[14] V. V. Khmelenko, H. Kunttu, and D. M. Lee, J. Low Temp. Phys. **148**, 1 (2007).
[15] R. E. Boltnev, E. P. Bernard, J. Jarvinen, V. V. Khmelenko, and D. M. Lee, Phys. Rev. B **79**, 180506 (2009).
[16] E. B. Gordon, L. P. Mezhov-Deglin, and O. F. Pugachev, JETP Lett. **19**, 63 (1974).
[17] S. I. Kiselev, V. V. Khmelenko, E. P. Bernard, and D. M. Lee, Low Temp. Phys. **29**, 505 (2003).
[18] E. B. Gordon, A. A. Pelmenev, O. F. Pugachev, and V. V. Khmelenko, Fizika Nizkikh Temperatur **11**, 563 (1985).
[19] G. T. Trammell, H. Zeldes, and R. Livingston, Phys. Rev. **110**, 630 (1958).
[20] T. Miyazaki, N. Iwata, K. Lee, and K. Fueki, J. Phys. Chem. **93**, 3352 (1989).
[21] A. S. Iskovskikh, A. Y. Katunin, I. I. Lukashevich, V. V. Sklyarevskii, V. V. Suraev, V. V. Filippov, N. I. Fillippov, and V. A. Shevtsov, Sov. Phys. JETP **64**, 1085 (1986).
[22] A. S. Iskovskikh, A. Y. Katunin, I. I. Lukashevich, V. V. Sklyarevskii, and V. A. Shevtsov, JETP Lett. **42**, 30 (1985).
[23] C. K. Jen, S. N. Foner, E. L. Cochran, and V. A. Bower, Phys. Rev. **104**, 846 (1956).
[24] P. Kusch, Phys. Rev. **100**, 1188 (1955).
[25] R. Beringer and M. A. Hearld, Phys. Rev. **95**, 1474 (1954).
[26] S. N. Foner, E. L. Cochran, V. A. Bower, and C. K. Jen, J. Chem. Phys. **32**, 963 (1960).
[27] V. V. Khmelenko, E. P. Bernard, S. Vasiliev, and D. M. Lee, Russ. Chem. Rev. **76**, 1107 (2007).
[28] K. Vaskonen, J. Eloranta, T. Kiljunen, and Kunttu, J. Chem. Phys. **110**, 2122 (1999).
[29] W. Gordy and R. Morehourse, Phys. Rev. **151**, 207 (1966).
[30] A. G. Prodell and P. Kusch, Phys. Rev. **88**, 184 (1952).
[31] C. K. Jen, S. N. Foner, E. L. Cochran, and V. A. Bowers, Phys. Rev. **112**, 1169 (1958).
[32] M. Sharnoff and P. V. Pound, Phys. Rev. **132**, 1003 (1963).
[33] L. B. Knight, W. E. Rice, L. Moore, E. R. Davidson, and R. S. Daily, J. Chem. Phys. **109**, 1409 (1998).
[34] T. Miyazaki, H. Morikita, K. Fueki, and T. Hiraku, Chem. Phys. Lett. **182**, 35 (1991).
[35] S. I. Kiselev, V. V Khmelenko, and D. M. Lee, J. Low Temp. Phys. **121**, 671 (2000).
[36] S. I. Kiselev, V. V Khmelenko, and D. M. Lee, Low Temp. Phys. **26**, 641 (2000).
[37] B. C. Crooker, B. Hebral, E. N. Smith, Y. Takano, and J. D. Reppy, Phys. Rev. Lett. **51**, 666 (1983).
[38] J. D. Reppy, B. C. Crooker, B. Hebral, A. D. Corwin, J. He, and G. M. Zassenhaus, Phys. Rev. Lett. **84**, 2060 (2000).
[39] E. B. Gordon, Dokl. Phys. Chem. **378**, 156 (2001).
[40] V. V. Khmelenko, D. M. Lee, and S. Vasiliev, J. Low Temp. Phys. **162**, 105 (2011).
[41] E. P. Bernard, V. V Khmelenko, and D. M. Lee, J. Low Temp. Phys. **150**, 516 (2008).
[42] S. Takayanagi, K. Nakamura, and S. Sato, J. Chem. Phys. **90**, 1641 (1989).
[43] T. Kumada, J. Chem. Phys. **124**, 094504 (2006).
[44] T. Kumada, M. Sakakibara, T. Nagasaka, H. Fukuta, J. Kumagai, and T. Miyazaki, J. Chem. Phys. **116**, 1109 (2002).
[45] V. Shevtsov, A. Scherbakov, P. Malmi, E. Ylinen, and M. Punkkinen, J. Low Temp. Phys. **104**, 211 (1996).
[46] T. Kumada, S. Mori, T. Nagasaka, J. Kumagai, and T. Miyazaki, J. Low Temp. Phys. **122**, 265 (2001).
[47] R. A. Zhitnikov, Yu. A. Dmitriev, and M. E. Kaimakov, Fizika Nizkikh Temperatur **15**, 367 (1989).
[48] B. R. Johnson, J. S. Denker, N. Bigelow, L. P. Levy, J. H. Freed, and D. M. Lee, Phys. Rev. Lett. **52**, 1508 (1984).
[49] S. Sheludiakov, J. Ahokas, O. Vainio, J. Jarvinen, D. Zvezdov, S. Vasiliev, V. V. Khmelenko, S. Mao, and D. M. Lee (unpublished).